5-7-2020

Gas Phase Protein Folding Triggered by Proton Stripping Generates Inside-Out Structures: A Molecular Dynamics Simulation Study.

Alexander I M Sever

Lars Konermann

Interrogating the Quaternary Structure of Noncanonical Hemoglobin Complexes by Electrospray Mass Spectrometry and Collision-Induced Dissociation

Alexander I. M. Sever, Victor Yin, and Lars Konermann*

Department of Chemistry, The University of Western Ontario, London, Ontario, N6A 5B7, Canada

* To whom correspondence should be addressed. E-mail: konerman@uwo.ca.

Funding was provided by the Natural Sciences and Engineering Research Council of Canada (RGPIN-2018-04243).

ABSTRACT: Various activation methods are available for the fragmentation of gaseous protein complexes produced by electrospray ionization (ESI). Such experiments can potentially yield insights into quaternary structure. Collision-induced dissociation (CID) is the most widely used fragmentation technique. Unfortunately, CID of protein complexes is dominated by the ejection of highly charged monomers, a process that does not yield any structural insights. Using hemoglobin (Hb) as a model system, this work examines under what conditions CID generates structurally informative subcomplexes. Native ESI mainly produced tetrameric Hb ions. In addition, "noncanonical" hexameric and octameric complexes were observed. CID of all these species [$(\alpha\beta)_2$, $(\alpha\beta)_3$, and $(\alpha\beta)_4$] predominantly generated highly charged monomers. In addition, we observed hexamer → tetramer + dimer dissociation, implying that hexamers have a tetramer··dimer architecture. Similarly, the observation of octamer → 2 tetramer dissociation revealed that octamers have a tetramer··tetramer composition. Gas phase candidate structures of Hb assemblies were produced by molecular dynamics (MD) simulations. Ion mobility spectrometry was used to identify the most likely candidates. Our data reveal that the capability of CID to produce structurally informative subcomplexes depends on the fate of protein-protein interfaces after transfer into the gas phase. Collapse of low affinity interfaces conjoins the corresponding subunits and favors CID via monomer ejection. Structurally informative subcomplexes are formed only if low affinity interfaces do not undergo a major collapse. However, even in these favorable cases CID is still dominated by monomer ejection, requiring careful analysis of the experimental data for the identification of structurally informative subcomplexes.

Introduction

Native electrospray ionization (ESI) [1] can transfer protein complexes into the gas phase as multiply charged ions that are amenable to mass spectrometry (MS). The resulting spectra reveal the subunit composition and ligand binding stoichiometry of the gaseous macroions [2-7]. The overall shape of electrosprayed proteins can be explored by combining ESI-MS with ion mobility spectrometry (IMS) [8-12].

Gas phase fragmentation experiments can yield additional insights into electrosprayed protein complexes, such as subunit connectivities in multi-protein complexes, the location of ligand binding sites, and sequence information. Techniques that have been applied in this context include electron capture and electron transfer dissociation [13-15], ultraviolet photodissociation [16,17], surface-induced dissociation (SID) [18], and blackbody-infrared dissociation [19]. Despite recent advances in the development of these and other methods [20,21], collision-induced dissociation (CID) remains the most widely used fragmentation technique [22-25]. The popularity of CID stems from the fact that it can be easily implemented on most mass spectrometers. During CID, analyte ions are electrostatically accelerated in the presence of a background gas. Collisional heating slowly increases the ion internal energy until, after some 10^4 or more collisions, dissociation takes place. For moderate collision energies only noncovalent bonds are disrupted, while higher energies also rupture covalent bonds [22-24]. In the following we focus on the former, specifically, the dissociation of protein complexes into their subunits.

CID has long been considered to be a promising avenue for extracting quaternary structural information, based on the expectation that the weakest subunit interfaces in multi-protein complexes should dissociate first [26,27]. For example, if a hypothetical complex consisting of subunits *abcd* preferentially produces *ab* and *cd* subcomplexes, one could conclude that *ab* and *cd* are closely linked, whereas other subunit contacts are much weaker (Figure 1A). In principle, CID

should therefore be able to uncover topological information such as subunit connectivities, and the placement of subunits inside vs. the periphery of a complex. This strategy has been successful in several cases [28,29].

Unfortunately, the formation of structurally informative subcomplexes during CID is not the dominant scenario. Instead, collisionally activated complexes predominantly eject monomers [30-38]. One might assume that a monomer that is ejected from an *n*-mer should carry roughly 1/*n* of the total charge. However, CID is accompanied by asymmetric charge partitioning (ACP) [30-34,39]. In this scenario the expelled monomer carries a disproportionally high charge. For example, 14+ streptavidin tetramers eject 7+ monomers, i.e., half the total charge is imparted on the monomeric product ion [34]. Experiments [32,35,36] and simulations [37,38] revealed that ACP is caused by the gradual unravelling of a single subunit, in conjunction with Coulombically driven migration of mobile protons onto this subunit. Ultimately, the subunit separates as a highly charged unfolded chain, leaving behind a charge-depleted (*n*-1)-mer (Figure 1B).

The predominance of ACP compromises the ability of CID to provide quaternary structural information, because complexes tend to undergo single-chain ejection regardless of their architecture [40,41]. One contributing factor to the information-poor nature of such CID data is the internal restructuring of protein complexes during collisional heating, a process that tends to erase native conformational features of prior to dissociation [35,36,38,40].

As a result of the aforementioned problem, the MS community has largely abandoned CID as a tool for interrogating the quaternary structure of protein complexes. Other approaches have become more popular. For example, SID can produce subcomplexes that retain a native-like topology, with preferential dissociation at the weakest subunit interfaces [18]. Also, topology information can be extracted from ESI-IMS/MS experiments conducted under mildly denaturing solution conditions where subunit connections are partially retained [42].

The current work revisits the CID behavior of protein complexes, taking a fresh look at the question whether such fragmentation data can yield quaternary structure information. We focus on bovine hemoglobin (Hb), a paradigmatic protein that consists of four heme-containing subunits (two α and two β chains) [43-46]. Hb has served as model system for numerous earlier native ESI-MS investigations [12,13,47-50]. Hb tetramers have a "dimer of dimers" quaternary structure, where one tightly bound αβ subcomplex interacts weakly with an identical second αβ subcomplex [51,52]. The four chains in Hb are referred to as α1, β1, α2, and β2 [53]. The interfacial buried surface area (IBSA) represents a measure of protein-protein binding affinity [54]. The high affinity α1-β1 and α2-β2 contacts each have an IBSA of 16.8 nm^2, much larger than the low affinity α1··β2 and α2··β1 contacts (IBSA = 10.0 nm^2) [55]. To account for the dimer of dimers architecture we denote Hb tetramers as $(\alpha\beta)_2$, rather than $\alpha_2\beta_2$. Consistent with this structure, Hb in solution shows a $(\alpha\beta)_2 \leftrightarrow 2\ (\alpha\beta)$ equilibrium [55-57]. This solution behavior is mirrored in native ESI mass spectra of Hb which are dominated by $(\alpha\beta)_2$ and αβ ions [12,13,47-49].

In addition to tetramers [i.e., $(\alpha\beta)_2$] and dimers [αβ], native ESI-MS of Hb also reveals the existence of larger "noncanonical" complexes, such as hexamers [$(\alpha\beta)_3$] and octamers [$(\alpha\beta)_4$] [47,49,58]. The origin of these noncanonical species has not been fully elucidated yet. It is possible that they form as clustering artifacts in shrinking ESI droplets prior to protein release into the gas phase [59,60], a scenario that is supported by pulsed hydrogen/deuterium exchange data [58]. Alternatively, the noncanonical assemblies might be derived from pre-existing complexes in solution. Flow rate or concentration-dependent measurements can sometimes help distinguish between these two scenarios [61]. Unfortunately, for the noncanonical Hb complexes considered here such experiments were inconclusive, because the abundance of the complexes is quite insensitive to the ESI conditions, e.g., nanoESI at 25 nL min^{-1} vs. regular ESI at 50 μL min^{-1} [62]. Raising the Hb concentration from 3 μM to 170 μM increases the abundance of the complexes

[62], but this effect is to be expected for both solution-phase binding and ESI clustering [63]. Hb from some animals [64,65] and after certain mutations (e.g., sickle cell Hb) [66] forms $(\alpha\beta)_n$ assemblies with $n > 2$ in solution. However, we are not aware of solution data on the presence of such larger species for wild-type mammalian Hb. Overall, it seems likely that the presence of noncanonical Hb complexes in native ESI mass spectra involves contributions from both scenarios, i.e., droplet clustering in combination with pre-existing weak solution contacts. Several other proteins show a similar behavior [15,39,67]. Regardless of their origin, noncanonical Hb assemblies represent an intriguing model system for studying fundamental aspects of protein complexes in the gas phase.

Here we performed CID experiments on Hb tetramers, hexamers, and octamers generated by native ESI. ACP ejection of monomers is the preferred dissociation mechanism for all three species. However, CID of hexamers and octamers also produced subcomplexes that report on the quaternary structures of the respective precursor ions. By complementing MS data with IMS experiments and molecular dynamics (MD) simulations we were able to delineate the necessary conditions under which CID generates fragments that provide insights into the subunit architecture of protein complexes.

Methods

Materials. Bovine Hb (64,479 Da) was prepared from hemolysate as described previously [49]. From its amino acid composition [55], the mass of Hb tetramers is 64,479 Da, corresponding to two α subunits (15053 Da), two β subunits (15954 Da), and four heme groups (616.2 Da). Neutral aqueous solutions were prepared containing 100 mM ammonium acetate and 60 μM Hb (as tetramer). ESI-MS studies on other protein complexes tend to use less concentrated (low μM)

solutions [2-7]. In the case of Hb, such low concentrations produce spectra that are dominated by [αβ] ions, consistent with a tetramer-dimer dissociation constant of ~2 μM [62]. 60 μM solutions were used here to boost the abundance of tetramers and larger noncanonical assemblies [62] which are the focus of our experiments. It is noted that 60 μM is still well below the ~5 mM concentration which represents the natural state of Hb in red blood cells [64]. Solutions for producing charge reduced Hb contained 2.5 mM or 10 mM triethylammonium acetate, and 5 mM ammonium acetate.

Mass Spectrometry and Ion Mobility Spectrometry. Mass spectra were acquired on a Synapt G2-Si instrument (Waters, Milford, MA). Hb solution was electrosprayed at +2.8 kV from a Z-spray ESI source at 5 μL min^{-1}. Experiments were performed with the cone set to 20 V, source temperature 25 °C, and desolvation temperature 40 °C. MS/MS was performed by trap cell CID with Ar as collision gas after quadrupole selection, and with trap collision voltages (referred to as "collision energy") of 30 to 70 V. IMS data were acquired on a Waters Synapt G2 using the same settings as noted above, except that the cone was lowered to 5 V to promote the preservation of solution structures. The transfer collision energy was set to 20 V to further desolvate ions after IMS. To promote the transmission of high mass ions the N_2 IMS flow was set to 35 mL min^{-1}, with an IMS wave height of 35 V and wave velocity of 500 m s^{-1}. Calibration of collision cross sections (**Ω**) followed established procedures [8], using a mix of reference proteins that were electrosprayed at pH 7 and in 200 mM ammonium acetate. Measured **Ω** values represent effective He collision cross sections. Error bars represent standard deviations of triplicate experiments on different days.

The dominant α and β monomeric CID products were in the heme-free state, reflecting the fact that heme in Hb is bound only through noncovalent contacts and a weak His coordination

bond [55]. Multi-subunit CID products retained their heme groups. To streamline the data presentation, we will avoid the designation of product ions as holo/apo except for a few instances.

Molecular Dynamics Simulations. Gas phase MD simulations were conducted using Gromacs 2018.4 [68], at 300 K without any truncation of nonbonded interactions [69]. The CHARMM36 force field [70] was used, partly, because it possesses predefined heme parameters that are essential for Hb simulations. More importantly, CHARMM36 has been proven to be effective for simulations that modeled the entire ESI process, from charged droplets to gaseous protein ions. The fidelity of those earlier modeling studies was supported by the agreement between experimental data and MD-derived parameters (charge states and Ω values) for a number of proteins [71]. The robustness of CHARMM36 for gas phase protein simulations has been further bolstered in recent work on the implications of force field overpolarization effects [72]. The X-ray data 2QSS [55] served as starting structure. Crystallographic neighbors were generated using the "generate symmetry mates within 4 Å" command in Pymol. Various hexamer and octamer starting arrangements were generated by selecting one central tetramer in conjunction with adjacent αβ or $(\alpha\beta)_2$ units. We used side chain titration patterns that maximized the zwitterionic character of the protein, consistent with experimental data [73]. For the initial MD stage these charges were chosen to obtain a net zero charge, followed by 100 ns of equilibration. For the subsequent 100 ns production runs the charges were adjusted to match the experimental values, i.e., tetramer^{17+}, hexamer^{23+}, and octamer^{27+}. These were implemented by neutralizing selected Asp and Glu, while leaving all Arg and Lys positive (His were neutral). He Ω values of MD structures were determined using Collidoscope [74] for the 80 ns, 90 ns, and 100 ns time points of the production runs. Protein interfaces were characterized by their IBSA values [54]. This was done by calculating solvent accessible surface areas (SASA) using the Gromacs gmx sasa routine with a

probe radius of 0.14 nm. For example, the IBSA of an α/β interface was calculated as IBSA(α/β) = SASA(α) + SASA(β) - SASA(αβ).

Results and Discussion

Hemoglobin ESI Mass Spectra. A native ESI mass spectrum of Hb is shown in Figure 2. Similar to previous studies [12,13,47-49] the data were dominated by $(\alpha\beta)_2$ and αβ ions, consistent with a tetramer-dimer equilibrium in solution [55-57]. In addition, the high *m/z* range of the spectrum revealed the presence of hexamers and octamers which represent noncanonical Hb assemblies [47,49,58]. The signal intensities of these noncanonical species were more than one order of magnitude lower than those of tetramers and dimers.

CID of Hb Complexes. Collisional activation of 19+ tetramers produced α and β monomers with charge states of 7+ to 11+, along with the complementary charge-depleted trimers

$$(\alpha\beta)_2^{z+} \rightarrow \alpha\beta_2^{(z-x)+} + \alpha^{x+} \quad (1)$$

$$(\alpha\beta)_2^{z+} \rightarrow \alpha_2\beta^{(z-x)+} + \beta^{x+} \quad (2)$$

with $x \approx z/2$ (Figure 3A). The charge states and signal intensities of α^{x+} and β^{x+} were similar, revealing that reactions 1 and 2 proceed with comparable kinetics. This behavior is consistent with the fact that α and β share similar structures and sequences, although β is slightly longer (145 vs. 141 residues) [55]. Trimers showed peak splitting due to heterogeneity in subunit stoichiometry ($\alpha_2\beta$ and $\alpha\beta_2$), and the presence/absence of excess heme (Figures 3A, S1). The CID data of Figure 3A represent a typical ACP scenario as previously reported for Hb [75,76] and many other complexes [30-38].

ACP behavior was also observed for hexamers. CID of 23+ hexamers produced highly charged α and β monomers along with the complementary charge-depleted pentamers. However, close inspection revealed the additional presence of tetramer and dimer fragment ions (Figure 3B), demonstrating the existence of a hexamer → tetramer + dimer dissociation pathway. This pathway suggests the presence a weak interface that is predisposed to dissociate after collisional activation, implying that hexamers have a $(\alpha\beta)_2\cdot\cdot(\alpha\beta)$ quaternary structure, i.e., a tetramer that is weakly bound to a dimer. The dots (··) in this notation represent the weak interface. Overall, CID of hexamers takes place via three competing reactions

$$(\alpha\beta)_2\cdot\cdot(\alpha\beta)^{z+} \rightarrow \alpha_2\beta_3^{(z-x)+} + \alpha^{x+} \quad (3)$$

$$(\alpha\beta)_2\cdot\cdot(\alpha\beta)^{z+} \rightarrow \alpha_3\beta_2^{(z-x)+} + \beta^{x+} \quad (4)$$

$$(\alpha\beta)_2\cdot\cdot(\alpha\beta)^{z+} \rightarrow (\alpha\beta)_2^{(z-y)+} + (\alpha\beta)^{y+} \quad (5)$$

The formation of highly charged α^{x+} and β^{x+} in reactions 3 and 4 represents the hallmark of ACP, implying that the monomers were ejected non-selectively and after extensive restructuring of the complex [30-34,39]. For this reason, reactions 3 and 4 do not yield any insights into the hexamer architecture. Only reaction (5) provides information on the quaternary structure of hexamers via the release of intact subcomplexes. The high specificity of reaction (5) is underlined by the fact that all of the dimeric fragments had an αβ composition, while neither α_2 nor β_2 ions were observed in Figure 3B. Similarly, trimeric fragment ions were absent.

Octamer CID data are displayed in Figure 3C. The collisionally activated 27+ ions primarily showed ACP behavior, with formation of highly charged monomers and charge-depleted heptamers. In addition, Figure 3C reveals a dissociation pathway where octamers dissociate into tetramers. This octamer → 2 tetramer dissociation strongly suggests that octamers have a $(\alpha\beta)_2\cdot\cdot(\alpha\beta)_2$ architecture, i.e., that they consist of two weakly bound tetramers. The absence of

dimeric fragments in Figure 3C renders other possible octamer structures such as $(\alpha\beta)\cdot\cdot(\alpha\beta)_2\cdot\cdot(\alpha\beta)$ extremely unlikely. The dissociation patterns of Figure 3C can be summarized by the reactions

$$(\alpha\beta)_2\cdot\cdot(\alpha\beta)_2{}^{z+} \rightarrow \quad \alpha_3\beta_4{}^{(z-x)+} \quad + \quad \alpha^{x+} \qquad (6)$$

$$(\alpha\beta)_2\cdot\cdot(\alpha\beta)_2{}^{z+} \rightarrow \quad \alpha_4\beta_3{}^{(z-x)+} \quad + \quad \beta^{x+} \qquad (7)$$

$$(\alpha\beta)_2\cdot\cdot(\alpha\beta)_2{}^{z+} \rightarrow \quad (\alpha\beta)_2{}^{(z-y)+} \quad + \quad (\alpha\beta)_2{}^{y+} \qquad (8)$$

The intact subcomplexes generated in reaction 8 provide information on the quaternary structure of the complex, i.e., the existence of a weak interface between the two tetramers that is prone to dissociation. The ACP reactions 6 and 7 do not yield any structural information.

In summary, collisional activation of Hb tetramers, hexamers, and octamers is dominated by ACP behavior (reactions 1-4, 6, 7). The highly charged monomers associated with these reactions represent the dominant signals in the CID spectra of Figure 3. Cursory analysis might suggest the absence of alternative pathways, in line with the purported information-poor nature of CID experiments on protein complexes [40,41]. Recognizing the occurrence of the structurally informative reactions 5 and 8 requires careful analysis of the spectra, because the dimeric and tetrameric fragments associated with these processes have relatively low intensities (Figure 3).

Monomer Charge States. The MS/MS data of Figure 3 were acquired with a collision energy of 40 V. It is interesting to examine how the CID products react to changes in collision energy. Monomer charge state distributions generated by CID of tetramers underwent only minor changes when the collision energy was ramped from 30 V to 60 V (Figure 4A-D). This invariance is not trivial because the collision energy could, in principle, alter charge state distributions by affecting the *m/z*-dependent ion transmission or by depleting high charge states via *b* and *y* ion formation

[77]. However, the control data (Figure 4A-D) reveal that CID-generated Hb monomers are not very susceptible to such effects in the energy range examined here.

In contrast to the data in Figure 4A-D, CID spectra of octamers exhibited a pronounced dependence on collision energy. CID spectra acquired at 30 V resulted in monomer charge states between 9+ and 13+, with a maximum at 11+ (Figure 4E). Upon raising the collision energy to 60 V these charge states were retained in the spectrum, but additionally the abundance of monomer charge states 7+ to 9+ increased dramatically. This effect caused significant broadening of the monomer charge state distribution, as well as a shift of the maximum from 11+ to 10+ (Figure 4H).

Considering the invariance of the control data in Figure 4A-D, the spectral changes in Figure 4E-H must be related to the CID behavior of octamers. The likely mechanism behind these changes is illustrated in Figure 4I: Octamer dissociation at 30 V proceeds via reactions 6-8; monomers in charge states 10+ to 13+ are the most abundant products under these conditions (Figure 4E-F). The tetramers formed in reaction 8 are quite stable due to their low charge states [77] (16+ down to 13+). However, upon raising the collision energy to 60 V the tetrameric CID products undergo secondary ACP dissociation. Second-generation monomers formed in this way have relatively low charge states (9+ to 7+) because they originate from low charge state tetramers (16+ to 13+). The 9+ to 7+ monomers formed in this way are responsible for broadening of the octamer CID spectrum at 60 V (Figure 4H). Our interpretation is supported by CID experiments on tetramers produced by ESI with charge reduction (Figure S4). Fragmentation of those species produced monomer charge states that depended on the tetramer charge. Specifically, 16+ to 13+ tetramers ejected 9+ to 7+ monomers, thereby bolstering the mechanism of Figure 4I.

Energy-dependent shifts in the charge states of monomeric fragments were also seen in CID experiments on hexamers (Figure S2). In analogy to the octamer dissociation of Figure 4E-I

we attribute shifts in the hexamer CID data to secondary tetramer (and possibly dimer) dissociation at elevated collision energies.

In summary, the energy-dependent shifts seen during CID of octamers (Figure 4E-H) and hexamers (Figure S2) are a telltale sign that helps confirm the existence of competing pathways during the fragmentation of protein complexes. One of these pathways is the ACP ejection of monomers, a process that does not provide any structural insights. The alternative to these ACP events is the formation of diagnostic CID products. This second pathway requires the dissociation along weak subunit interfaces, producing subcomplexes that report on the quaternary structure of the macroions. The latter is exemplified by the dissociation of $(\alpha\beta)_2{\cdot\cdot}(\alpha\beta)$ and $(\alpha\beta)_2{\cdot\cdot}(\alpha\beta)_2$ via reactions 5 and 8. The subcomplexes generated in this way can undergo secondary dissociation when the collision energy is raised, ejecting single chains that shift the overall monomer spectrum toward lower charge states (Figures 3E-H, S2).

Ion Mobility Spectrometry and Structural Modeling. Native ESI-IMS/MS of tetramers, hexamers, and octamers yielded Ω distributions with maxima of 38.6, 55.7, and 67.5 nm^2, (Figure 5A), with standard deviations of less than 1 %. These data confirm the expected size progression of the three species, i.e., tetramer < hexamer < octamer [50]. When considered in isolation these experimental data provide only limited insights, because any given Ω value is compatible with a multitude of conformations [78,79]. Similar to previous studies [79-82], we addressed this ambiguity by using MD simulations for generating gas phase candidate structures.

MD runs were conducted at ambient temperature (300 K) to probe the gas phase protein behavior under the gentle conditions of native ESI experiments. Starting from Hb X-ray data [55] (Figure 6A) we used 100 ns MD runs to generate nine gas phase tetramer conformations that had an average Ω of 40.4 nm^2 (Figure 5B).

Identifying suitable starting structures for hexamer and octamer MD runs was less straightforward because these noncanonical assemblies have not been characterized previously. However, in Hb crystals each tetramer is closely surrounded by many other $(\alpha\beta)_2$ units (Figure 6C). This crystal packing reveals favorable interchain contacts, providing clues to possible assembly motifs beyond the canonical $(\alpha\beta)_2$ structure [83]. As noted earlier, the formation of Hb hexamer and octamer ions may reflect pre-existing solution contacts and/or clustering in the shrinking ESI droplets. The crystal interchain contacts provide reasonable starting points for both scenarios, because even ESI-generated clusters settle into well-defined free energy minima (e.g., magic number complexes [84,85]) instead of forming random conglomerates. Accordingly, we used the Hb crystal packing to generate hexamer starting structures by selecting one $(\alpha\beta)_2$ along with different adjacent αβ units (20 unique coordinate sets). Analogously, octamers were produced by selecting pairs of adjacent $(\alpha\beta)_2$ units (5 unique coordinate sets).

Gas phase MD of these complexes, with the appropriate ESI charge states, produced a host of structures. The Ω distributions of these MD structures were wide and multimodal (Figure 5B). Comparison with the experimental peak maxima revealed that not all of the MD structures were suitable candidates (dashed lines in Figure 5B). To select the most appropriate species we filtered tetramer/hexamer/octamer MD structures by only retaining those within 1 nm^2 of the experimental Ω values. This filtering resulted in the retention of 2/9 tetramers, 11/60 hexamers, and 6/15 octamer structures (see examples in Figure 6B, D, E). By design, these MD conformations had Ω distributions that agreed closely with the experimental IMS data (Figure 5C). The species highlighted in Figure 6B, D, E represent likely candidate structures for the gaseous ions formed under the conditions of our work. However, the existence of alternative assembly motifs cannot be ruled out, keeping in mind that experimental **Ω** value are relatively information-poor as they represent a single number that may be compatible with various structures [78,79].

CID Behavior is Governed by Gas Phase Quaternary Structure. Our MD data help to elucidate the conditions that have to be met for CID to produce structurally informative subcomplexes. As discussed above, these analytically desirable dissociation events are in kinetic competition with the information-poor ACP ejection of monomers.

The crystal structure of Hb tetramers reveals a dimer of dimers structure consisting of four subunits that are referred to as α1, β1, α2, and β2 (see Introduction) [51-53]. The α1β1··α2β2 interface represents the weakest contact in native Hb (IBSA = 26.3 nm^2, Figure 6A) [55]. Why does CID of tetramers fail to produce dimers via rupture of this interface? Our MD data showed that tetramers undergo structural rearrangement in the gas phase, including the collapse of cavities at the α1β1··α2β2 interface. This collapse caused the IBSA of this interface to increase dramatically (to 58 ± 4 nm^2, Figure 6B). Thus, contacts along this interface are substantially strengthened after ESI [54]. Similar compaction events have been reported for other gas phase proteins [82,86-88]. Strengthening of the α1β1··α2β2 interface in the gas phase reduces the likelihood of α1β1··α2β2 → α1β1 + α2β2 dissociation after collisional activation. Instead, CID of tetramers proceeds with ACP ejection of α and β monomers (reactions 1, 2).

Gas phase collapse of the α1β1··α2β2 interface also occurred for hexamers and octamers, resulting in IBSA values of 61 ± 5 nm^2 and 65 ± 4 nm^2 (Figure 6D, E). In contrast, the noncanonical interfaces in hexamers and octamers retained a much looser connectivity, evident from their smaller IBSA values of 36 ± 6 nm^2 and 38 ± 7 nm^2. Visual inspection of the dumbbell-shaped gas phase structures immediately reveals the locations of these weak interfaces [see the constrictions between the tetramer/dimer (Figure 6D), and between the two tetramers (Figure 6E)]. The low IBSAs of these noncanonical interfaces increase the likelihood of dissociation into structurally informative subcomplexes. As a result, reactions 5, 8 can kinetically compete with the

ACP ejection of monomers. Collapse of the noncanonical interfaces may be hampered by their relatively nonselective and heterogeneous nature. This is in contrast to the natural α1β1··α2β2 interface which has a multitude of specific contacts [43-46], that favor collapse in the gas phase.

Conclusions

Previous studies have painted a somewhat unclear picture as to whether CID of noncovalent protein assemblies can produce structurally informative subcomplexes [26-29], or whether CID should be avoided because it is dominated by ACP monomer ejection [40,41]. The latter pathway involves extensive structural changes prior to dissociation, such that the ejection of monomers does not imply that these subunits were loosely bound in the native state [35,36,38,40]. The current work confirms earlier reports [28,29] that CID can nonetheless yield quaternary structural information by generating structurally informative subcomplexes (Figure 1a). However, this approach is viable only in certain cases. The chances of learning about subunit connectivities depend on the preservation of low affinity interfaces in the gas phase that act as fracture-prone "fault lines", and that preferentially dissociate during ion activation. The current work contributes to a better understanding under what conditions such a scenario is viable.

Our data demonstrate that the presence of a weak protein-protein interface in solution does *not* guarantee preferential dissociation of this interface in the gas phase. Instead, weak interfaces may collapse and undergo significant strengthening in the gas phase [82,86-88]. Such a scenario is encountered for Hb tetramers (Figure 6A,B). Although the Hb tetramer crystal structure represents a prototypical dimer-of-dimers architecture [51,52,55], collapse of the dimer-dimer interface generates sticky contacts that prevent tetramer → 2 dimer dissociation during CID. As a result, Hb

tetramers only undergo ACP monomer ejection which does not yield insights into quaternary structure.

In contrast to the aforementioned scenario, Hb hexamers and octamers were identified as having $(\alpha\beta)_2\cdot\cdot(\alpha\beta)$ and $(\alpha\beta)_2\cdot\cdot(\alpha\beta)_2$ quaternary structures. The dots in this notation represent low affinity interfaces that *retain* a low affinity after transitioning into the gas phase (Figure 6D, E). These rupture-prone contacts allow the release of structurally informative subcomplexes. For example, the $(\alpha\beta)_2\cdot\cdot(\alpha\beta)_2$ quaternary structure of octamers was deduced from the observation of reaction 8 (octamer → 2 tetramers). We did not see any dissociation according to octamer → tetramer + 2 dimers, which would have indicated a $(\alpha\beta)\cdot\cdot(\alpha\beta)_2\cdot\cdot(\alpha\beta)$ composition. Despite the occurrence of structurally informative dissociation events (reactions 5 and 8), most of the Hb hexamers and octamers still undergo ACP monomer ejection. These non-informative ACP events are prevalent because collisional heating promotes the loss of native structure prior to dissociation [35,36,38,40]. As a result, dissociation along structurally informative interfaces is in kinetic competition with ACP monomer ejection.

Overall, this work demonstrates that CID of protein complexes can be a viable approach for obtaining quaternary structural information. Recognizing the presence of structurally informative subcomplexes after CID requires careful analysis of the spectra, because important low intensity product ions may go unnoticed upon cursory inspection. Whether or not CID produces diagnostic subcomplexes depends on the extent to which collapse events restructure protein-protein interfaces after transfer into the gas phase. Despite the versatility of other ion activation methods [20,41,89-91], it is comforting that classical CID measurements remain a core utensil in the mass spectrometrist's toolbox for numerous applications, including the interrogation of protein complexes.

References

1. Fenn, J.B.: Electrospray Wings for Molecular Elephants (Nobel Lecture). *Angew. Chem. Int. Ed.* **42,** 3871-3894 (2003)

2. Leney, A.C., Heck, A.J.R.: Native Mass Spectrometry: What is in the Name? *J. Am. Soc. Mass Spectrom.* **28,** 5-13 (2017)

3. Mehmood, S., Allison, T.M., Robinson, C.V.: Mass Spectrometry of Protein Complexes: From Origins to Applications. *Annu. Rev. Phys. Chem.* **66,** 453-474 (2015)

4. Loo, J.A.: Electrospray Ionization Mass Spectrometry: a Technology for Studying Noncovalent Macromolecular Complexes. *Int. J. Mass Spectrom.* **200,** 175-186 (2000)

5. Sharon, M.: Structural MS Pulls Its Weight. *Science* **340,** 1059-1060 (2013)

6. Erba, E.B., Signor, L., Petosa, C.: Exploring the structure and dynamics of macromolecular complexes by native mass spectrometry. *J. Proteomics* **222,** 17 (2020)

7. Chen, F., Gulbakan, B., Weidmann, S., Fagerer, S.R., Ibanez, A.J., Zenobi, R.: Applying mass spectrometry to study non-covalent biomolecule complexes. *Mass Spectrom. Rev.* **35,** 48-70 (2016)

8. Bush, M.F., Hall, Z., Giles, K., Hoyes, J., Robinson, C.V., Ruotolo, B.T.: Collision Cross Sections of Proteins and Their Complexes: A Calibration Framework and Database for Gas-Phase Structural Biology. *Anal. Chem.* **82,** 9667-9565 (2010)

9. Wyttenbach, T., Pierson, N.A., Clemmer, D.E., Bowers, M.T.: Ion Mobility Analysis of Molecular Dynamics. *Annu. Rev. Phys. Chem.* **65,** 175–196 (2014)

10. Jurneczko, E., Barran, P.E.: How useful is ion mobility mass spectrometry for structural biology? The relationship between protein crystal structures and their collision cross sections in the gas phase. *Analyst* **136,** 20-28 (2011)

11. Woods, L.A., Radford, S.E., Ashcroft, A.E.: Advances in ion mobility spectrometry-mass spectrometry reveal key insights into amyloid assembly. *Biochim. Biophys. Acta* **1834,** 1257-68 (2013)

12. Woodall, D.W., Brown, C.J., Raab, S.A., El-Baba, T.J., Laganowsky, A., Russell, D.H., Clemmer, D.E.: Melting of Hemoglobin in Native Solutions as measured by IMS-MS. *Anal. Chem.* **92,** 3440-3446 (2020)

13. Cui, W.D., Zhang, H., Blankenship, R.E., Gross, M.L.: Electron-capture dissociation and ion mobility mass spectrometry for characterization of the hemoglobin protein assembly. *Protein Sci.* **24,** 1325-1332 (2015)

14. Lermyte, F., Konijnenberg, A., Williams, J.P., Brown, J.M., Valkenborg, D., Sobott, F.: ETD Allows for Native Surface Mapping of a 150 kDa Noncovalent Complex on a Commercial Q-TWIMS-TOF Instrument. *J. Am. Soc. Mass Spectrom.* **25,** 343-350 (2014)

15. Li, H.L., Nguyen, H.H., Ogorzalek Loo, R.R., Campuzano, I.D.G., Loo, J.A.: An integrated native mass spectrometry and top-down proteomics method that connects sequence to structure and function of macromolecular complexes. *Nat. Chem.* **10,** 139-148 (2018)

16. Morrison, L.J., Brodbelt, J.S.: 193 nm Ultraviolet Photodissociation Mass Spectrometry of Tetrameric Protein Complexes Provides Insight into Quaternary and Secondary Protein Topology. *J. Am. Chem. Soc.* **138,** 10849-10859 (2016)

17. Hendricks, N.G., Julian, R.R.: Leveraging ultraviolet photodissociation and spectroscopy to investigate peptide and protein three-dimensional structure with mass spectrometry. *Analyst* **141,** 4534-4540 (2016)

18. Harvey, S.R., Seffernick, J.T., Quintyn, R.S., Song, Y., Ju, Y., Yan, J., Sahasrabuddhe, A.N., Norris, A., Zhou, M.W., Behrman, E.J., Lindert, S., Wysocki, V.H.: Relative interfacial cleavage energetics of protein complexes revealed by surface collisions. *Proc. Natl. Acad. Sci. U. S. A.* **116,** 8143-8148 (2019)

19. Felitsyn, N., Kitova, E.N., Klassen, J.S.: Thermal Decomposition of a Gaseous Multiprotein Complex Studied by Blackbody Infrared Radiative Dissociation. Investigating the Origin of the Asymmetric Dissociation Behavior. *Anal. Chem.* **73,** 4647-4661 (2001)

20. Brodbelt, J.S.: Ion Activation Methods for Peptides and Proteins. *Anal. Chem.* **88,** 30-51 (2016)

21. Zhou, M.W., Liu, W.J., Shaw, J.B.: Charge Movement and Structural Changes in the Gas-Phase Unfolding of Multimeric Protein Complexes Captured by Native Top-Down Mass Spectrometry. *Anal. Chem.* **92,** 1788-1795 (2020)

22. McLuckey, S.A., Goeringer, D.E.: Slow heating methods in tandem mass spectrometry. *J. Mass Spectrom.* **32,** 461-474 (1997)

23. Sleno, L., Volmer, D.A.: Ion activation methods for tandem mass spectrometry. *J. Mass Spectrom.* **39,** 1091-1112 (2004)

24. Mayer, P.M., Poon, C.: The Mechanism of Collisional Activation of Ions in Mass Spectrometry. *Mass Spectrom. Rev.* **28,** 608-639 (2009)

25. Yin, S., Xie, Y., Loo, J.A.: Mass Spectrometry of Protein-Ligand Complexes: Enhanced Gas-Phase Stability of Ribonuclease-Nucleotide Complexes. *J. Am. Soc. Mass Spectrom.* **19,** 1199-1208 (2008)

26. Benesch, J.L.P., Aquilina, J.A., Ruotolo, B.T., Sobott, F., Robinson, C.V.: Tandem Mass Spectrometry Reveals the Quaternary Organization of Macromolecular Assemblies. *Chem. Biol.* **13,** 597-605 (2006)

27. Ilag, L.L., Videler, H., McKay, A.R., Sobott, F., Fucini, P., Nierhaus, K.H., Robinson, C.V.: Heptameric (L12)(6)/L10 rather than canonical pentameric complexes are found by tandem MS of intact ribosomes from thermophilic bacteria. *Proc. Natl. Acad. Sci. U. S. A.* **102,** 8192-8197 (2005)

28. Erba, E.B., Ruotolo, B.T., Barsky, D., Robinson, C.V.: Ion Mobility-Mass Spectrometry Reveals the Influence of Subunit Packing and Charge on the Dissociation of Multiprotein Complexes. *Anal. Chem.* **82,** 9702-9710 (2010)

29. Hall, Z., Hernández, H., Marsh, J.A., Teichmann, S.A., Robinson, C.V.: The Role of Salt Bridges, Charge Density, and Subunit Flexibility in Determining Disassembly Routes of Protein Complexes. *Structure* **21,** 1325-1337 (2013)

30. Mistarz, U.H., Chandler, S.A., Brown, J.M., Benesch, J.L.P., Rand, K.D.: Probing the Dissociation of Protein Complexes by Means of Gas-Phase H/D Exchange Mass Spectrometry. *J. Am. Soc. Mass Spectrom.* **30,** 45-57 (2019)

31. Madsen, J.A., Brodbelt, J.S.: Asymmetric charge partitioning upon dissociation of DNA duplexes. *J. Am. Soc. Mass Spectrom.* **21,** 1144-1150 (2010)

32. Jurchen, J.C., Williams, E.R.: Origin of Asymmetric Charge Partitioning in the Dissociation of Gas-Phase Protein Homodimers. *J. Am. Chem. Soc.* **125,** 2817-2826 (2003)

33. Ogorzalek Loo, R.R., Loo, J.A.: Salt Bridge Rearrangement (SaBRe) Explains the Dissociation Behavior of Noncovalent Complexes. *J. Am. Soc. Mass Spectrom.* **27,** 975-990 (2016)

34. Schwartz, B.L., Bruce, J.E., Anderson, G.A., Hofstadler, S.A., Rockwood, A.L., Smith, R.D., Chilkoti, A., Stayton, P.S.: Dissociation of Tetrameric Ions of Noncovalent Streptavidin Complexes Formed by Electrospray Ionization. *J. Am. Soc. Mass Spectrom.* **6,** 459-465 (1995)

35. Ruotolo, B.T., Hyung, S.-J., Robinson, P.M., Giles, K., Bateman, R.H., Robinson, C.V.: Ion Mobility–Mass Spectrometry Reveals Long-Lived, Unfolded Intermediates in the Dissociation of Protein Complexes. *Angew. Chem. Int. Ed.* **46,** 8001-8004 (2007)

36. Quintyn, R.S., Zhou, M., Yan, J., Wysocki, V.H.: Surface-Induced Dissociation Mass Spectra as a Tool for Distinguishing Different Structural Forms of Gas-Phase Multimeric Protein Complexes. *Anal. Chem.* **87,** 11879-11886 (2015)

37. Fegan, S.K., Thachuk, M.: A Charge Moving Algorithm for Molecular Dynamics Simulations of Gas-Phase Proteins. *J. Chem. Theory Comput.* **9,** 2531-2539 (2013)

38. Popa, V., Trecroce, D.A., McAllister, R.G., Konermann, L.: Collision-Induced Dissociation of Electrosprayed Protein Complexes: An All-Atom Molecular Dynamics Model with Mobile Protons. *J. Phys. Chem. B* **120,** 5114-5124 (2016)

39. Abzalimov, R.R., Frimpong, A.K., Kaltashov, I.A.: Gas-phase processes and measurements of macromolecular properties in solution: On the possibility of false positive and false negative signals of protein unfolding. *Int. J. Mass Spectrom.* **253,** 207-216 (2006)

40. Benesch, J.L.P.: Collisional Activation of Protein Complexes: Picking Up the Pieces. *J. Am. Soc. Mass Spectrom.* **20,** 341-348 (2009)

41. Wysocki, V.H., Jones, C.M., Galhena, A.S., Blackwell, A.E.: Surface-Induced Dissociation Shows Potential to Be More Informative Than Collision-Induced Dissociation for Structural Studies of Large Systems. *J. Am. Soc. Mass Spectrom.* **19,** 903-913 (2008)

42. Taverner, T., Hernandez, H., Sharon, M., Ruotolo, B.T., Matak-Vinkovic, D., Devos, D., Russell, R.B., Robinson, C.V.: Subunit Architecture of Intact Protein Complexes from Mass Spectrometry and Homology Modeling. *Acc. Chem. Res.* **41,** 617-627 (2008)

43. Eaton, W.A., Henry, E.R., Hofrichter, J., Mozzarelli, A.: Is cooperative oxygen binding by hemoglobin really understood. *Nat. Struct. Biol.* **6,** 351 - 358 (1999)

44. Perutz, M.F., Wilkinson, A.J., Paoli, M., Dodson, G.G.: The stereochemical mechanism of the cooperative effects in hemoglobin revisited. *Annu. Rev. Biophys. Biomolec. Struct.* **27,** 1-34 (1998)

45. Dey, S., Chakrabarti, P., Janin, J.: A survey of hemoglobin quaternary structures. *Proteins* **79,** 2861-2870 (2011)

46. Bellelli, A., Brunori, M.: Hemoglobin allostery: Variations on the theme. *Biochim. Biophys. Acta* **1807,** 1262-1272 (2011)

47. Griffith, W.P., Kaltashov, I.A.: Highly asymmetric interactions between globin chains during hemoglobin assembly revealed by electrospray ionization mass spectrometry. *Biochemistry* **42,** 10024 - 10033 (2003)

48. Scarff, C.A., Patel, V.J., Thalassinos, K., Scrivens, J.H.: Probing Hemoglobin Structure by Means of Traveling-Wave Ion Mobility Mass Spectrometry. *J. Am. Soc. Mass Spectrom.* **20,** 625-631 (2009)

49. Boys, B.L., Kuprowski, M.C., Konermann, L.: Symmetric Behavior of Hemoglobin α- and β- Subunits during Acid-Induced Denaturation Observed by Electrospray Mass Spectrometry. *Biochemistry* **46,** 10675-10684 (2007)

50. Kang, Y., Terrier, P., Douglas, D.J.: Mass Spectra and Ion Collision Cross Sections of Hemoglobin. *J. Am. Soc. Mass Spectrom.* **22,** 290-299 (2011)

51. Ackers, G.K., Holt, J.M.: Asymmetric cooperativity in a symmetric tetramer: Human hemoglobin. *J. Biol. Chem.* **281,** 11441-11443 (2006)

52. Alcantara, R.E., Xu, C., Spiro, T.G., Guallar, V.: A quantum-chemical picture of hemoglobin affinity. *Proc. Natl. Acad. Sci. U.S.A.* **104,** 18451-18455 (2007)

53. Dickerson, R.E., Geis, I. *Hemoglobin: Structure, Function, Evolution, and Pathology*; The Benjamin/Cummings Publishing Company, Inc.: Menlo Park, CA, 1983.

54. Chen, J.M., Sawyer, N., Regan, L.: Protein-protein interactions: General trends in the relationship between binding affinity and interfacial buried surface area. *Protein Sci.* **22,** 510-515 (2013)

55. Aranda IV, R., Cai, H., Worley, C.E., Levin, E.J., Li, R., Olson, J.S., Phillips Jr, G.N., Richard, M.P.: Structural analysis of fish versus mammalian hemoglobins: Effect of the heme pocket enviornment on autooxidation and hemin loss. *Proteins* **75,** 217-230 (2009)

56. Atha, D.H., Riggs, A.: Tetramer-Dimer Dissociation in Hemoglobin and the Bohr Effect. *J. Biol. Chem.* **251,** 5537-5543 (1976)

57. Huang, Y.X., Wu, Z.J., Huang, B.T., Luo, M.: Pathway and Mechanism of pH Dependent Human Hemoglobin Tetramer-Dimer-Monomer Dissociations. *PLoS One* **8,** 9 (2013)

58. Hossain, B.M., Konermann, L.: Pulsed hydrogen/deuterium exchange MS/MS for studying the relationship between noncovalent protein complexes in solution and in the gas phase after electrospray ionization. *Anal. Chem.* **78,** 1613-1619 (2006)

59. Kitova, E.N., El-Hawiet, A., Schnier, P.D., Klassen, J.S.: Reliable Determinations of Protein–Ligand Interactions by Direct ESI-MS Measurements. Are We There Yet? *J. Am. Soc. Mass Spectrom.* **23,** 431-441 (2012)

60. Peschke, M., Verkerk, U.H., Kebarle, P.: Features of the ESI Mechanism that Affect the Observation of Multiply Charged Noncovalent Protein Complexes and the Determination of the Association Constant by the Titration Method. *J. Am. Soc. Mass Spectrom.* **15,** 1424-1434 (2004)

61. Reardon, P.N., Jara, K.A., Rolland, A.D., Smith, D.A., Hoang, H.T.M., Prell, J.S., Barbar, E.J.: The dynein light chain 8 (LC8) binds "in-register" to multivalent intrinsically disordered partners. *J. Biol. Chem.* **295,** 4912–4922 (2020)

62. Liu, J., Konermann, L.: Protein-Protein Binding Affinities In Solution Determined by Electrospray Mass Spectrometry. *J. Am. Soc. Mass Spectrom.* **22,** 408-417 (2011)

63. Benesch, J.L.P., Ruotolo, B.T., Simmons, D.A., Robinson, C.V.: Protein Complexes in the Gas Phase: Technology for Structural Genomics and Proteomics. *Chem. Rev.* **107,** 3544-3567 (2007)

64. Riggs, A.F.: Self-association, cooperativity and supercooperativity of oxygen binding by hemoglobins. *J. Exper. Biol.* **201,** 1073-1084 (1998)

65. Royer, W.E., Zhu, H., Gorr, T.A., Flores, J.F., Knapp, J.E.: Allosteric hemoglobin assembly: Diversity and similarity. *J. Biol. Chem.* **280,** 27477-27480 (2005)

66. Manning, J.M., Dumoulin, A., Li, X.F., Manning, L.R.: Normal and abnormal protein subunit interactions in hemoglobins. *J. Biol. Chem.* **273,** 19359-19362 (1998)

67. van Berkel, W.J.H., van den Heuvel, R.H.H., Versluis, C., Heck, A.J.R.: Detection of intact megaDalton protein assemblies of vanillyl-alcohol oxidase by mass spectrometry. *Protein Sci.* **9,** 435-439 (2000)

68. Abraham, M.J., Murtola, T., Schulz, R., Páll, S., Smith, J.C., Hess, B., Lindahl, E.: GROMACS: High performance molecular simulations through multi-level parallelism from laptops to supercomputers. *SoftwareX* **1–2,** 19-25 (2015)

69. Konermann, L., Metwally, H., McAllister, R.G., Popa, V.: How to run molecular dynamics simulations on electrospray droplets and gas phase proteins: Basic guidelines and selected applications. *Methods* **144,** 104-112 (2018)

70. Huang, J., MacKerell, A.D.: CHARMM36 all-atom additive protein force field: Validation based on comparison to NMR data. *J. Comput. Chem.* **34,** 2135-2145 (2013)

71. Konermann, L., Metwally, H., Duez, Q., Peters, I.: Charging and Supercharging of Proteins for Mass Spectrometry: Recent Insights into the Mechanisms of Electrospray Ionization. *Analyst* **144,** 6157-6171 (2019)

72. Lee, J.H., Pollert, K., Konermann, L.: Testing the Robustness of Solution Force Fields for MD Simulations on Gaseous Protein Ions. *J. Phys. Chem. B* **123,** 6705-6715 (2019)

73. Bonner, J.G., Lyon, Y.A., Nellessen, C., Julian, R.R.: Photoelectron Transfer Dissociation Reveals Surprising Favorability of Zwitterionic States in Large Gaseous Peptides and Proteins. *J. Am. Chem. Soc.* **139,** 10286-10293 (2017)

74. Ewing, S.A., Donor, M.T., Wilson, J.W., Prell, J.S.: Collidoscope: An Improved Tool for Computing Collisional Cross-Sections with the Trajectory Method. *J. Am. Soc. Mass Spectrom.* **28,** 587-596 (2017)

75. Sciuto, S.V., Liu, J., Konermann, L.: An Electrostatic Charge Partitioning Model for the Dissociation of Protein Complexes in the Gas Phase. *J. Am. Soc. Mass Spectrom.* **22,** 1679-1689 (2011)

76. Chernushevich, I.V., Loboda, A.V., Thomson, B.A.: An introduction to quadrupole time-of-flight mass spectrometry. *J. Mass Spectrom.* **36,** 849 - 865 (2001)

77. Thomson, B.A.: Declustering and Fragmentation of Protein Ions from an Electrospray Ion Source. *J. Am. Soc. Mass Spectrom.* **8,** 1053-1058 (1997)

78. Eschweiler, J.D., Frank, A.T., Ruotolo, B.T.: Coming to Grips with Ambiguity: Ion Mobility-Mass Spectrometry for Protein Quaternary Structure Assignment. *J. Am. Soc. Mass Spectrom.* **28,** 1991-2000 (2017)

79. Gabelica, V., Marklund, E.: Fundamentals of ion mobility spectrometry. *Curr. Op. Chem. Biol.* **42,** 51-59 (2017)

80. Mao, Y., Ratner, M.A., Jarrold, M.F.: Molecular Dynamics Simulations of the Charge-Induced Unfolding and Refolding of Unsolvated Cytochrome c. *J. Phys. Chem. B* **103,** 10017-10021 (1999)

81. Albrieux, F., Calvo, F., Chirot, F., Vorobyev, A., Tsybin, Y.O., Lepère, V., Antoine, R., Lemoine, J., Dugourd, P.: Conformation of polyalanine and polyglycine dications in the gas phase: insight from ion mobility spectrometry and replica-exchange molecular dynamics. *J. Phys. Chem. A* **114,** 6888-6896 (2010)

82. Rolland, A.D., Prell, J.S.: Computational insights into compaction of gas-phase protein and protein complex ions in native ion mobility-mass spectrometry. *Trac-Trends Anal. Chem.* **116,** 282-291 (2019)

83. Rodriguez, A.D., Dunn, S.D., Konermann, L.: ATP-Induced Dimerization of the FOF1 Epsilon Subunit from Bacillus PS3: A Hydrogen Exchange/Mass Spectrometry Study. *Biochemistry* **53,** 4072-4080 (2014)

84. Zhang, D.X., Cooks, R.G.: Doubly charged cluster ions (NaCl)(m)(Na)(2) (2+): magic numbers, dissociation, and structure. *Int. J. Mass Spectrom.* **195,** 667-684 (2000)

85. Scutelnic, V., Perez, M.A.S., Marianski, M., Warnke, S., Gregor, A., Rothlisberger, U., Bowers, M.T., Baldauf, C., von Helden, G., Rizzo, T.R., Seo, J.: The Structure of the Protonated Serine Octamer. *J. Am. Chem. Soc.* **140,** 7554-7560 (2018)

86. Jhingree, J.R., Bellina, B., Pacholarz, K.J., Barran, P.E.: Charge Mediated Compaction and Rearrangement of Gas-Phase Proteins: A Case Study Considering Two Proteins at Opposing Ends of the Structure-Disorder Continuum. *J. Am. Soc. Mass Spectrom.* **28,** 1450-1461 (2017)

87. Devine, P.W.A., Fisher, H.C., Calabrese, A.N., Whelan, F., Higazi, D.R., Potts, J.R., Lowe, D.C., Radford, S.E., Ashcroft, A.E.: Investigating the Structural Compaction of Biomolecules Upon Transition to the Gas-Phase Using ESI-TWIMS-MS. *J. Am. Soc. Mass Spectrom.* **28,** 1855-1862 (2017)

88. Hall, Z., Politis, A., Bush, M.F., Smith, L.J., Robinson, C.V.: Charge-State Dependent Compaction and Dissociation of Protein Complexes: Insights from Ion Mobility and Molecular Dynamics. *J. Am. Chem. Soc.* **134,** 3429-3438 (2012)

89. Syka, J.E.P., Coon, J.J., Schroeder, M.J., Shabanowitz, J., Hunt, D.F.: Peptide and protein sequence analysis by electron transfer dissociation mass spectrometry. *Proc. Natl. Acad. Sci. U.S.A.* **101,** 9528-9533 (2004)

90. Zubarev, R.A., Kelleher, N.L., McLafferty, F.W.: Electron Capture Dissociation of Multiply Charged Protein Cations. A Nonergodic Process. *J. Am. Chem. Soc.* **120,** 3265-3266 (1998)

91. Yoo, H.J., Wang, N., Zhuang, S.Y., Song, H.T., Hakansson, K.: Negative-Ion Electron Capture Dissociation: Radical-Driven Fragmentation of Charge-Increased Gaseous Peptide Anions. *J. Am. Chem. Soc.* **133,** 16790-16793 (2011)

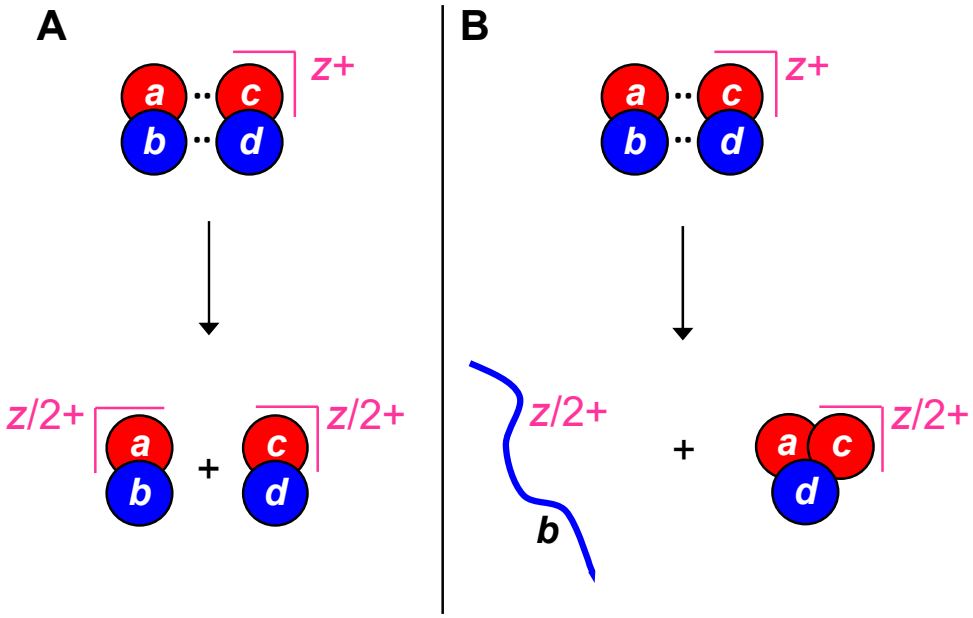

Figure 1. Possible CID scenarios for a hypothetical protein complex with subunits *a*, *b*, *c*, *d*. (A) The weak *ab*··*cd* interface favors dissociation into *ab* and *cd* subcomplexes. This dissociation pathway yields insights into the quaternary structure of the complex, i.e., it reveals the presence of tight contacts between subunits *a* and *b*, as well as *c* and *d*. (B) Asymmetric charge partitioning (ACP) causes the ejection of a highly charged unfolded monomer (subunit *b*). This dissociation reaction does not provide any insights into the quaternary structure of the complex.

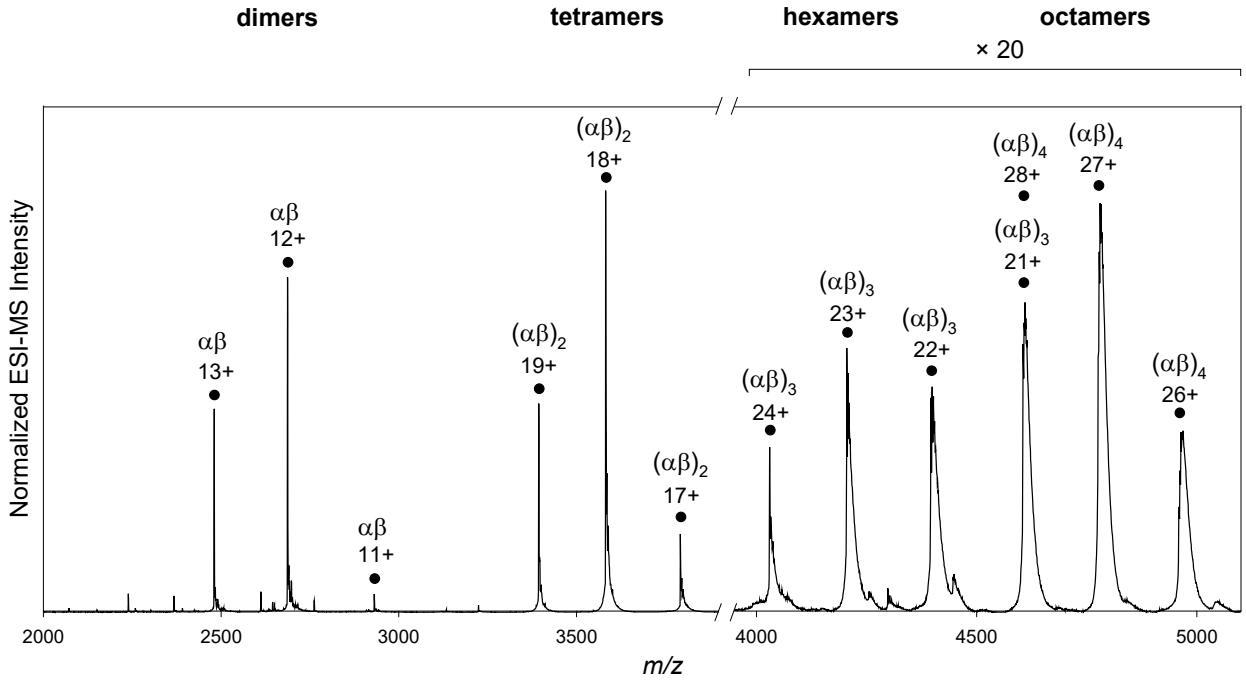

Figure 2. Native ESI mass spectrum of Hb. Different protein complexes are annotated according to their α/β subunit composition and charge state. Dots indicate expected peak positions calculated from the known subunit masses. Intensities at high *m*/*z* are magnified by a factor of twenty.

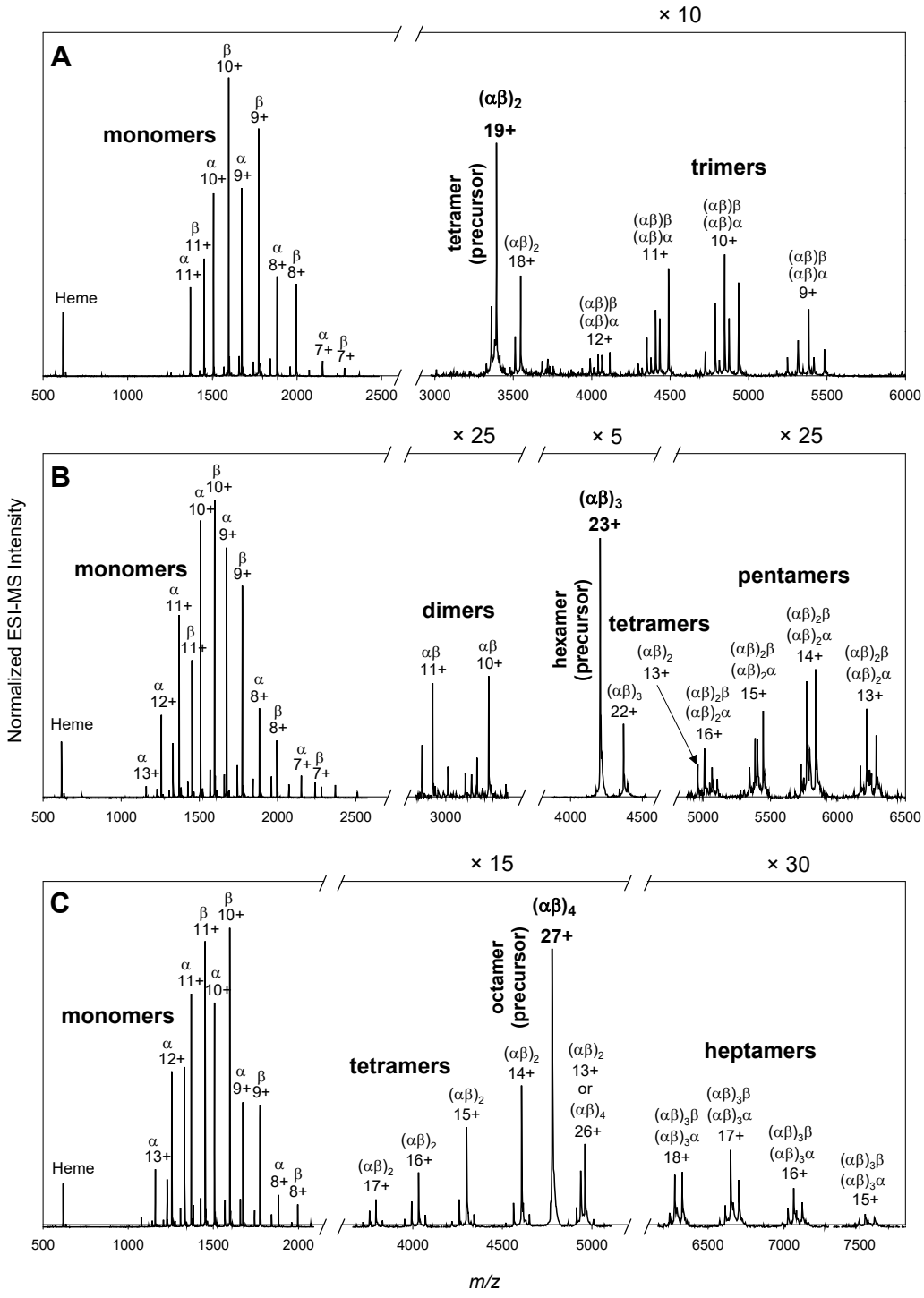

Figure 3. CID tandem mass spectra of different Hb complexes at a collision energy of 40 V. The residual precursor ion signal is indicated in each spectrum: (A) 19+ tetramer, (B) 23+ hexamer, and (C) 27+ octamer. Product ions are indicated as monomers, dimers, trimers, tetramers, pentamers, and heptamers. For additional details (e.g., peak splitting caused by heme loss), see Figure S1.

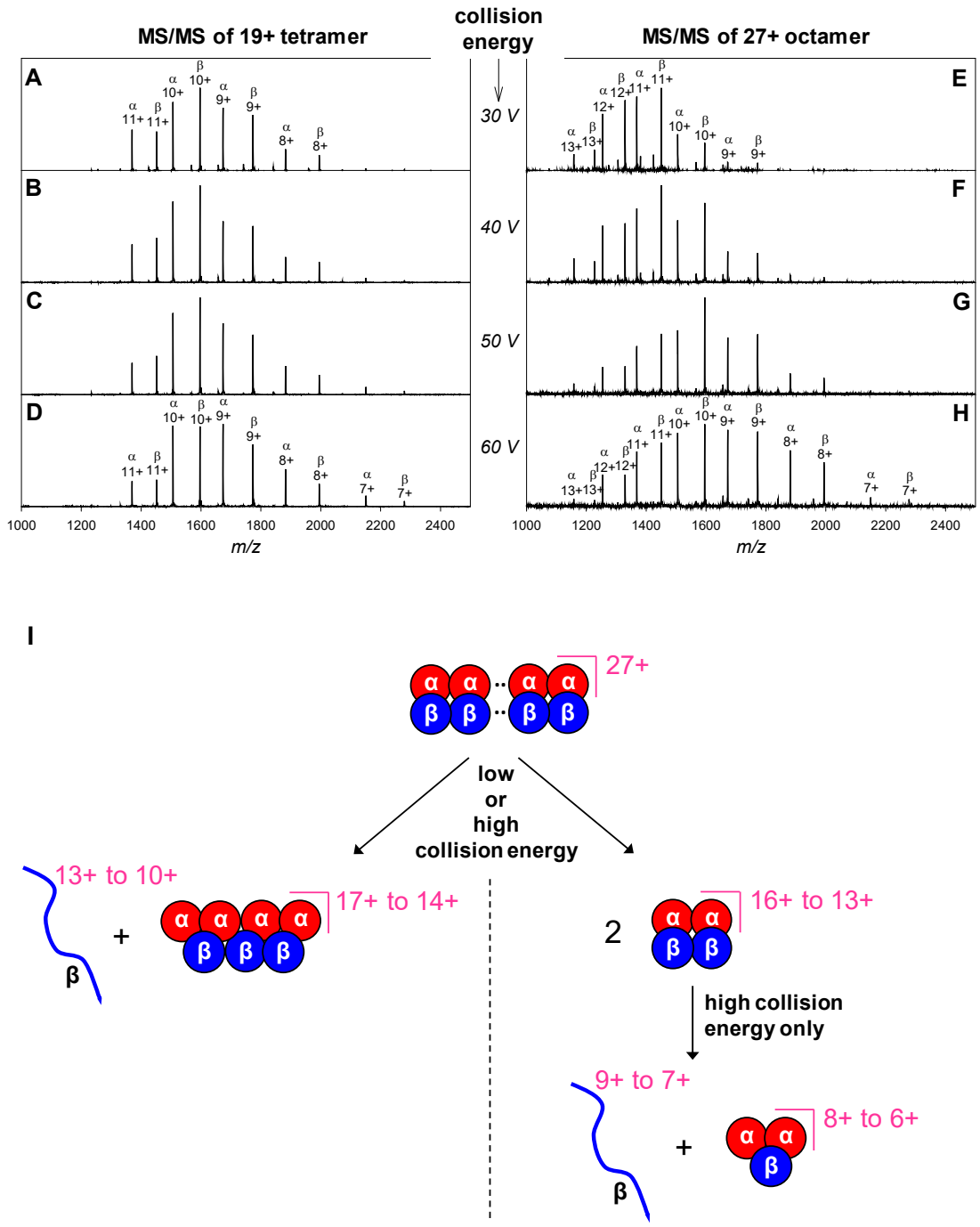

Figure 4. Monomeric fragment ions obtained after CID of 19+ tetramers (A-D) and 27+ octamers (E-H) at different collision energies. The corresponding hexamer data are shown in Figure S2; full spectra are shown in Figure S3. (I) Reaction scheme for octamer fragmentation at low (30 V) and high (60 V) collision energy. Low energy produces highly charged monomers (left branch), whereas high energy additionally generates low charge monomers via secondary fragmentation of tetramers (right branch). Although the cartoon only shows ejection of β monomers, ejection of α monomers takes place with the same probability.

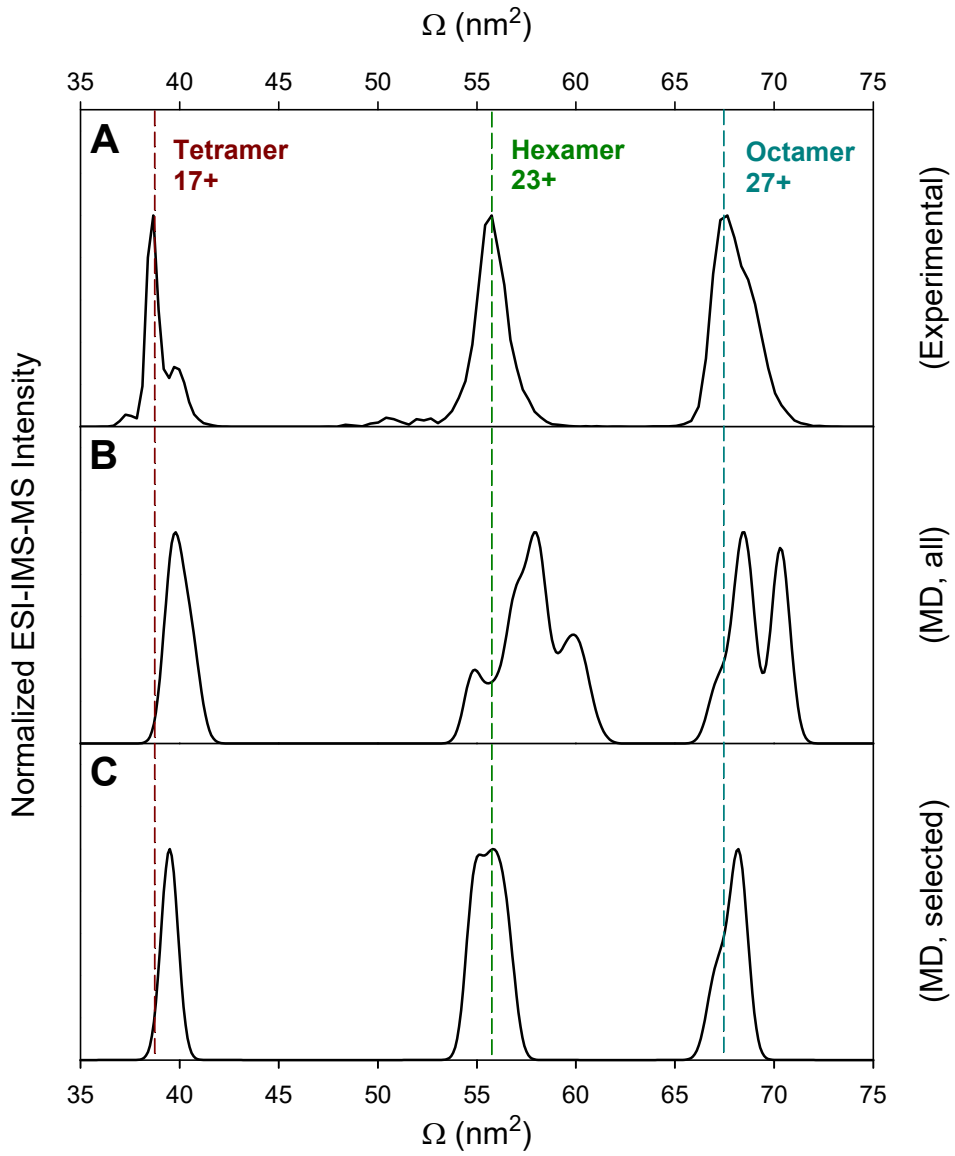

Figure 5. (A) Experimental IMS data for Hb tetramers, hexamers, and octamers. Dashed lines indicate experimental peak maxima. (B) Calculated cumulative IMS distributions of all MD structures, prior to filtering. The calculated values were convoluted with a Gaussian (FWHM = 1 nm^2) to approximate the experimental IMS resolution. (C) Same as in panel B, but for only those MD structures within 1 nm^2 of the experimental maxima.

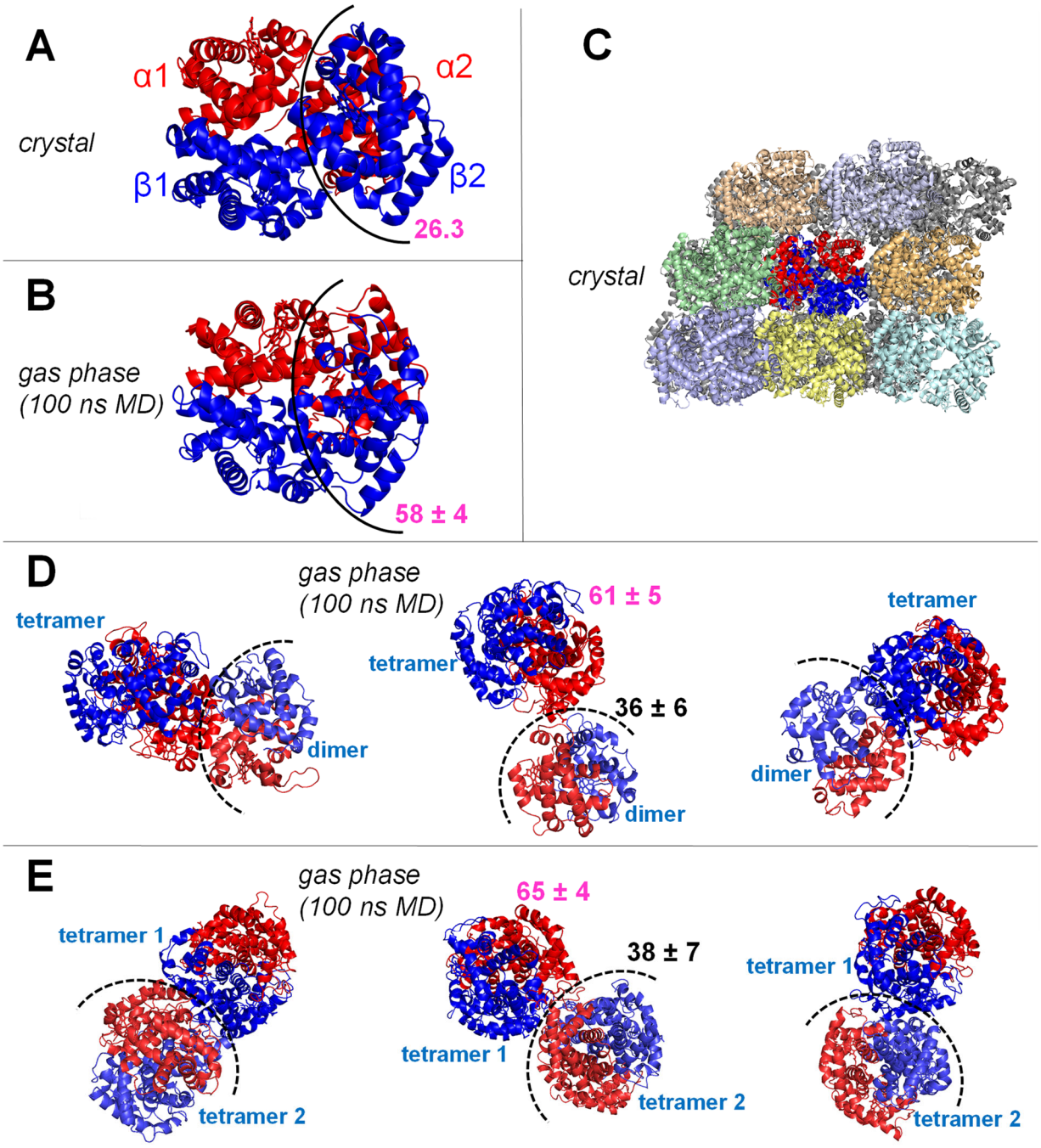

Figure 6. (A) Hb crystal structure 2qss [55] with α and β subunits (red/blue). The arc indicates the weak α1β1··α2β2 interface. (B) Same as in panel A, but after 100 ns of gas phase MD, charge state 17+. (C) Hb crystal structure, where one $(\alpha\beta)_2$ (red/blue) is surrounded by other $(\alpha\beta)_2$ units. One $(\alpha\beta)_2$ facing the observer was removed for visualization. (D) MD structures of 23+ hexamers. (E) MD structures of 27+ octamers. Purple numbers are interfacial buried surface areas (IBSA, in nm^2) of the α1β1··α2β2 interface. Dashed lines indicate experimentally observed CID fracture interfaces (reactions 5, 8) with their IBSA values (black). Structures in B, D, E were filtered as outlined in Figure 5C.

For Table of Contents Only

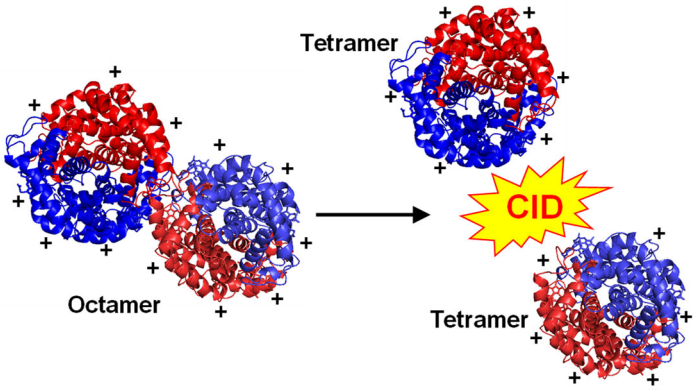

Interrogating the Quaternary Structure of Noncanonical Hemoglobin Complexes by Electrospray Mass Spectrometry and Collision-Induced Dissociation

Alexander I. M. Sever, Victor Yin, and Lars Konermann*

Synopsis: Under certain conditions CID can produce structurally informative subcomplexes from electrosprayed multi-protein assemblies.